NACE INTERNATIONAL

CORROSION
Conference & Expo 2019

Study of Phase Distribution on Alloy UNS N07718 in Different Hardening Conditions and Its Relationship with Hydrogen Embrittlement Susceptibility

Julia Botinha
VDM Metals International GmbH
Plettenbergerstrasse 2
58791 Werdohl
Germany

Bodo Gehrmann
VDM Metals International GmbH
Plettenbergerstrasse 2
58791 Werdohl
Germany

Helena Alves
VDM Metals International GmbH
Plettenbergerstrasse 2
58791 Werdohl
Germany

Ralph Gilles
Technische Universität München
Heinz Maier-Leibnitz Zentrum (MLZ)
Lichtenbergstrasse 1
85748 Garching
Germany

Cecilia Solís
Technische Universität München
Heinz Maier-Leibnitz Zentrum (MLZ)
Lichtenbergstrasse 1
85748 Garching
Germany

Johannes Munke
Technische Universität München
Heinz Maier-Leibnitz Zentrum (MLZ)
Lichtenbergstrasse 1
85748 Garching
Germany

Artem Feoktystov
Forschungszentrum Jülich GmbH
Jülich Centre for Neutron Science at MLZ
Lichtenbergstrasse 1
85748 Garching
Germany

Volodymyr Baran
Forschungsneutronenquelle Heinz Maier-Leibnitz
Technische Universität München
Lichtenbergstrasse 1
85748 Garching
Germany

ABSTRACT

The precipitation-hardenable Nickel Alloy UNS[1] N07718 is one of the most commonly applied alloy in the oil and gas industry. Enriched with amounts of niobium, molybdenum, titanium and aluminum, this alloy is known as having good corrosion resistance in sour gas applications while presenting excellent strength properties.

---

[1] Unified Numbering System for Metals and Alloys (UNS), SAE International, Warrendale, PA

The austenitic matrix of γ phase is strengthened by the intermetallic precipitates γ' (ordered fcc Ni3Al phase) and γ'' (bcc tetragonal Ni3Nb phase). Co-precipitates can also be observed.

Studies have been carried out in order to compare and better understand the hydrogen embrittlement resistance of three different aging conditions of N07718. The interaction of hydrogen with the microstructure has been evaluated by means of hydrogen embrittlement susceptibility tests and structural characterization by neutron diffraction and small-angle neutron scattering technique.

Key words: UNS N07718, Alloy 718, precipitation hardening, hydrogen embrittlement, phase composition, neutron diffraction (ND), small-angle neutron scattering (SANS), slow strain rate tensile (SSRT)

INTRODUCTION

Due to the good corrosion resistance combined with its excellent strength properties, the precipitation-hardenable Nickel Alloy UNS N07718 is one of the most preferred applied alloys in the oil and gas industry. In order to achieve the desired properties, this alloy is enriched with amounts of niobium, molybdenum, titanium and aluminum. However, the reported hydrogen embrittlement susceptibility can be a serious limit to the material application.[1,2]

The austenitic matrix of γ phase is strengthened by the intermetallic precipitates γ' (ordered fcc Ni_3Al phase) and γ'' (bcc tetragonal Ni_3Nb phase). Co-precipitates can also be observed. The existence of the different phases and their quantities and shapes depend on composition, heat treatment and processing conditions. In order to tailor the mechanical and corrosion properties in application environments, the control of their evolution is crucial.

For several years, the susceptibility to hydrogen embrittlement of the Alloy 718 was attributed to the δ-phase precipitation.[3,4] Recent studies show that the strengthening phases (γ' and γ'') can also play an important role on the corrosion resistance of the alloy.[5-8] Gosheva et al.[9] have made important contributions to clarify the impact of microstructure on the hydrogen embrittlement susceptibility of N07718. Their studies concluded that the amount of hydrogen stored at the material during cathodical hydrogen charging was predominantly dependent on the strengthening precipitates and their interface with the γ matrix. Klapper et al.[10] showed that the presence of precipitates, rather than the strength or hardness level, predominantly affect the hydrogen embrittlement (HE) susceptibility and define the type of embrittlement mechanism. These results make the study of the phase distribution, as well as the particle size distribution, very important for the understanding of the interaction of the hydrogen with the material, when comparing different material conditions and their corrosion behavior.

With this aim, different samples of Alloy 718 after different hardening heat treatments (between 600°C and 800°C) were analyzed. The interaction of hydrogen with the microstructure was evaluated by means of hydrogen embrittlement susceptibility tests and structural characterization by neutron diffraction (ND) and small-angle neutron scattering (SANS) technique.

Small-angle neutron scattering technique is used to study precipitates or voids sizes and morphologies in the range of 10 – 3000 Å.[11] Neutron powder diffraction technique is used to reveal information on the phase composition of a sample and the structural details of the present phases.[12]

EXPERIMENTAL PROCEDURE

Material

Three different VAR (Vacuum Arc Remelting) commercial heats from the same VIM (Vacuum Induction Melting) melt were produced. These three heats are designated A, B and C and their nominal chemical composition is shown in **Table 1**.The ingots were homogenized and forged to 203.2 mm (8 inch) round bars, which were posteriorly solution annealed and age hardened. The bar from the first ingot,

denominated A, was age hardened under the standard ageing temperature range defined by the API[2] 6A CRA[13] to produce a minimum 120 ksi yield strength material. The bar coming from the second ingot, denominated B, was age hardened under a lower temperature that is responsible for optimizing the mechanical properties (to produce a minimum 140 ksi yield strength material) and the third bar C, under a two-step heat treatment, that gives to the material improved mechanical properties (minimum 150 ksi yield strength) when compared to the single-step heat treatment. Heat treatment parameters are summarized and given by **Table 2**.

Table 1
Nominal chemical composition of heats of Alloy UNS N07718 and API 6A CRA composition requirements in percentage mass fraction (% wt.)

Element	Heat designation			API 6A CRA requirements	
	A	B	C	min	max
Ni	54.69	54.39	53.84	50	55
Cr	18.55	18.61	18.59	17	21
Fe	16.97	17.25	17.84		Bal.
Nb	5.00	4.97	4.93	-	-
Nb+Ta				4.87	5.2
Mn	0.03	0.03	0.04		0.35
Si	0.08	0.08	0.09		0.35
Mo	3.07	3.05	3.03	2.8	3.3
Ti	0.96	0.94	0.93	0.8	1.15
P	0.005	0.005	0.005		0.01
Al	0.47	0.51	0.54	0.4	0.6
C	0.014	0.012	0.012		0.045
Co	0.06	0.06	0.05		1
B	0.004	0.004	0.004		0.006
S	0.0005	<0.0005	0.0006		0.01

Table 2
Heat treatment parameters of bars A B and C of Alloy UNS N07718

Sample designation	Material grade	Heat treatment					
		Solution Annealing					
		Temperature, °C (°F)	holding time, h	Cooling rate, °C/h (°F/h)	Temperature, °C (°F)	Holding time, h	Cooling media
A, B, C	-	1032 (1890)	1	-	-	-	Water
		Age hardening					
A	120K	790 (1454)	7	-	-	-	Air
B	140K	760 (1400)	8	-	-	-	Air
C	150K	720 (1328)	8	50 (122)	620 (1148)	8	Air

Microstructure

Microstructural investigations were carried out on representative samples of bars A, B and C. The specimens were mechanically polished and chemically etched in pickling solution (100mL H2O, 100mL HCl and 10mL HNO3). Evaluation was performed using optical and scanning electron microscopy (SEM) techniques. The samples were analyzed by using an optical microscope at 100X and 500X magnification and SEM at 50,000X magnification. The grain sizes were measured according to ASTM[3] E112[14].

Hydrogen Embrittlement Susceptibility Tests

In order to evaluate the hydrogen embrittlement (HE) susceptibility of the given material grades, slow strain rate tensile (SSRT) tests were performed in two different laboratories, using two different test configurations, which will be called Test 1 and Test 2. The analysis of the results are also different and attention must be paid when a comparison is made.

Test Configuration 1

Standard SSRT test specimens complying with NACE[4] TM0198-201626[15] with gauge section diameter of 3.81 mm (0.15-in) and gauge section length of 25.5 mm (1-in) were used. For each grade of material, one specimen was tested in control environment, which consists of distilled water purged with nitrogen, and three specimens were tested in aggressive environment, which consists of 0.5 M sulfuric acid solution with applied cathodic current density of 5 mA·cm^{-2} to obtain cathodic polarization. Water was selected as control environment due to the easiness of its use and the possibility of having a better temperature control. No reaction is expected between water and the material surface. Both solutions were maintained at 40°C (104°F) during the tests and the specimen was submitted to a strain rate of 1x10^{-6} s^{-1} (crosshead speed 2.5x10^{-5} mm·s^{-1}). Time-to-failure, reduction-of-area and elongation-to-failure are reported and the ratios between aggressive and control environments are calculated.
A set threshold of 45% of elongation-to-failure-ratio is used to qualify the material as acceptable or not acceptable against hydrogen embrittlement[16]. Results greater than the 45% are considered accepted and the higher the elongation-to-failure-ratio, the less the susceptibility of a material to hydrogen embrittlement.
All of the specimens were inspected using light microscopy to determine the presence of secondary cracking after testing.

Test Configuration 2

For the evaluation of the hydrogen embrittlement susceptibility of the given material grades, slow tensile tests were performed at the displacement rate of 0.02 mm·h^{-1} under continuous cathodic hydrogen charging at room temperature (23 °C, 73.4°F). The chosen displacement rate is supposed to match approximately the strain rate of 10^{-6} s^{-1}, which is recommended in NACE TM 0177[17] specification. The tests were performed both in air (control medium) and in 1.0 M (NH4)2SO4 solution having pH 3 (H2SO4) under the constant cathodic current density of 30 mA·cm^{-2} (aggressive medium). Round notched (notch factor αK=4.2) tensile specimens were used. Self-adhesive galvanic tape was applied to assure the consistent ratio between the sample surface and the volume of the tested electrolyte, as shown in **Figure 1**.

---

[3] American Society for Testing and Materials (ASTM) International, 100 Barr Harbor Drive, West Coshohocken, PA, 19428
[4] National Association of Corrosion Engineers (NACE) International, 15835 Park Ten Place, Houston, TX 77084

Figure 1: Round notched tensile specimen with self-adhesive galvanic tape prior to the test

Hydrogen embrittlement susceptibility of the material grades was evaluated according to the value of the hydrogen embrittlement coefficient (HE) with the expression given in (1), where l_H is the elongation of the hydrogenated sample and l_A is the elongation of the sample tested in air.

$$HE\ (\%) = \left(1 - \frac{l_H}{l_A}\right) . 100 \tag{1}$$

The accepting criteria defined for this test configuration is that the material must have a hydrogen embrittlement coefficient smaller than 50%[18]. The lower the hydrogen embrittlement coefficient, the lower the hydrogen embrittlement susceptibility of the material.

All of the specimens were inspected using SEM microscopy to determine the fracture surface.

Neutron Scattering Techniques

Flat squared samples of 15x15 mm and 0.8 mm thicknesses (of each material grade – Heats A, B and C) were investigated by SANS at RT. The measurements were performed at the KWS-1 instrument[19] at the Heinz Maier-Leibnitz Zentrum (MLZ). The neutron wavelength λ of 0.5 nm was used and the sample to detector distance (SDD) was varied from 1.5 to 20 m. With these settings, the modulus of scattering vector Q had a range from 0.03 to 4 nm^{-1}. QtiKWS program[20] was used for the treatment of the obtained raw data which were corrected for background scattering and calibrated to absolute scale by additional measurements of 1.5 mm-thick flat piece of poly(methyl methacrylate) (PMMA)[19].

Neutron diffraction (ND) measurements were performed in Debye-Scherrer geometry for phase analysis at RT using the high-resolution powder diffractometer SPODI at MLZ.[22,23] Neutrons with a wavelength λ of 0.1548 nm from the Ge (551) monochromator were incident on the cylindrical probes of 6 mm in diameter and 40 mm in length. For minimization of the preferred orientation effect on the diffraction pattern, the sample placed into a thin-wall (0.15 mm) vanadium can of 7 mm in diameter, was constantly rotated during data collection. Each sample was measured for 4 h. The data evaluation of diffractograms was performed with Rietveld refinement[24] using the Fullprof software[25].

RESULTS

Microstructure

Microstructure images made by using an optical microscope of the three bars of Alloy 718 in the different age-hardening conditions are shown in **Figure 2**. The microstructure is consistent with the API 6A CRA requirements, showing an austenitic matrix with equiaxed grain structure and no duplex grain size. The measured grain size is ASTM No. 6 in average.

Scanning Electron Microscopy (SEM) images of etched specimens of similar material that was manufactured in the same production route of bars A, B and C with similar chemical composition were performed and are represented in **Figure 3**. The phases are pointed out on the image of samples from Heat A and B, due to the biggest size of particles, that allows the identification.

The δ phase (white needle-like precipitates in Figure 3) could be identified at the grain boundaries only in the SEM investigation. According to the API 6A CRA, the acceptance criteria for metallographic examinations for deleterious phases shall be made at 100X and 500X using light microscopy and at this magnification the δ phase precipitates could not be seen, what leads to the acceptance of the material. The tiny particles distributed in the matrix are determined as γ' (point-type) and metastable γ'' (line

shape). The reduction of age-hardening temperature leads, as expected, to smaller precipitate sizes, which are responsible for strengthening the material.
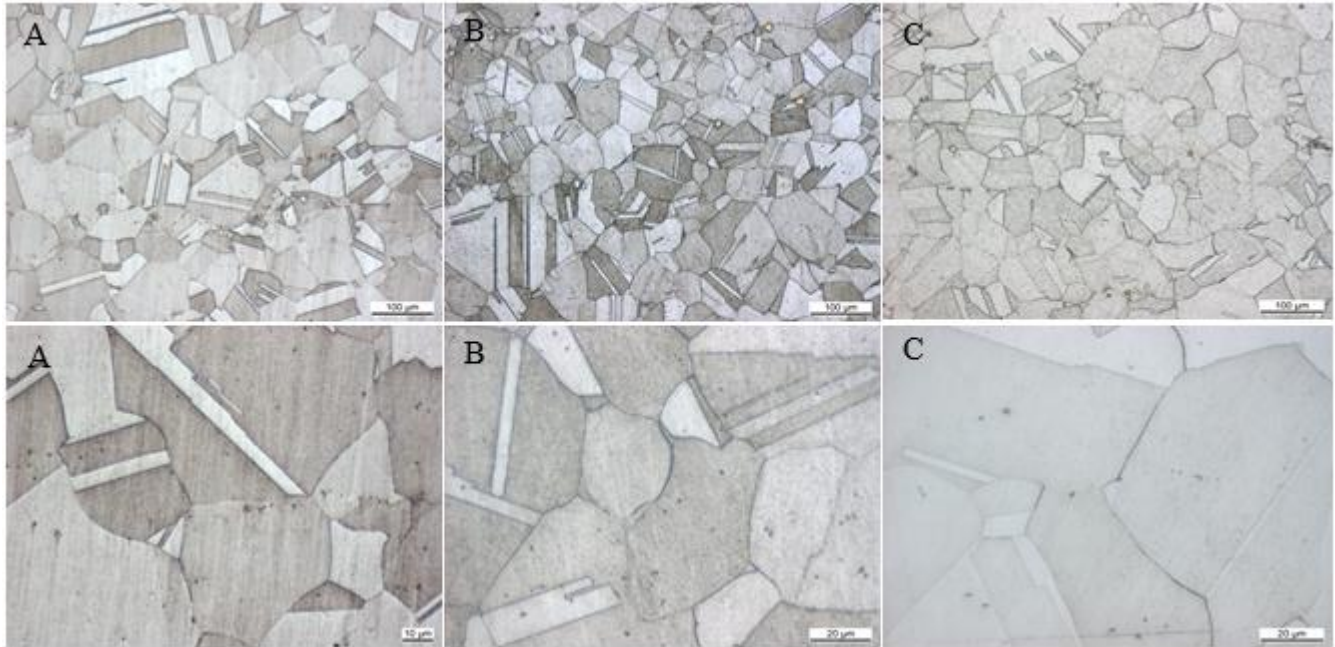
Figure 2: Typical microstructure of the three bars of Alloy 718 in the different heat treatment conditions, A B and C at 100x and 500x magnification.
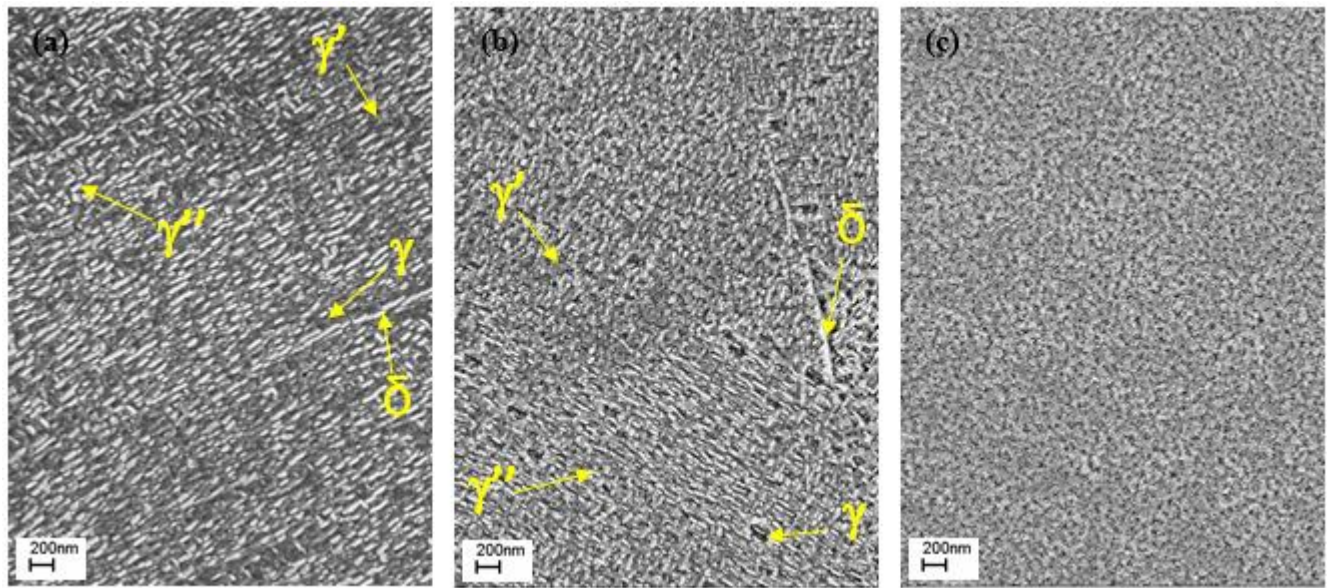
Figure 3: SEM micrographs of similar material corresponding to bars A (a), B (b) and C (c), respectively. Specimens etched with V2A; 50,000X Magnification.

Corrosion Testing

Test Configuration 1

The susceptibility to HE of the three grades of the Alloy UNS N07718 was evaluated by means of SSRT. When comparing the ductility parameters determined for samples tested in aggressive environment with those of samples tested in control (inert) environment, ductility ratios are determined

and are used to rate the resistance to environmental crack. A value of 45% elongation-to-failure ratio is a set threshold for classifying precipitation-hardened nickel alloys with respect to its susceptibility to HE and values close to 100% indicate that the material does not suffer influence of the aggressive media. The lower the elongation-to-failure ratio, the higher the sensitivity to hydrogen embrittlement.

The three studied material grades of Alloy UNS N07718 present good resistance to HE, as can be concluded from the elongation-to-failure ratios that are well above the threshold of 45%.

Figure 4 shows that the heat C (150K material designation) presents the highest elongation-to-failure ratio (92%) and the best resistance to HE. This sample is followed by the Heat A (120K material designation) that shows an elongation-to-failure ratio of 75%, and lastly by the Heat B (140K Material Designation) that shows elongation-to-failure ratio of 66%.

Detailed SSRT results from test configuration 1 are summarized in **Table 3**.
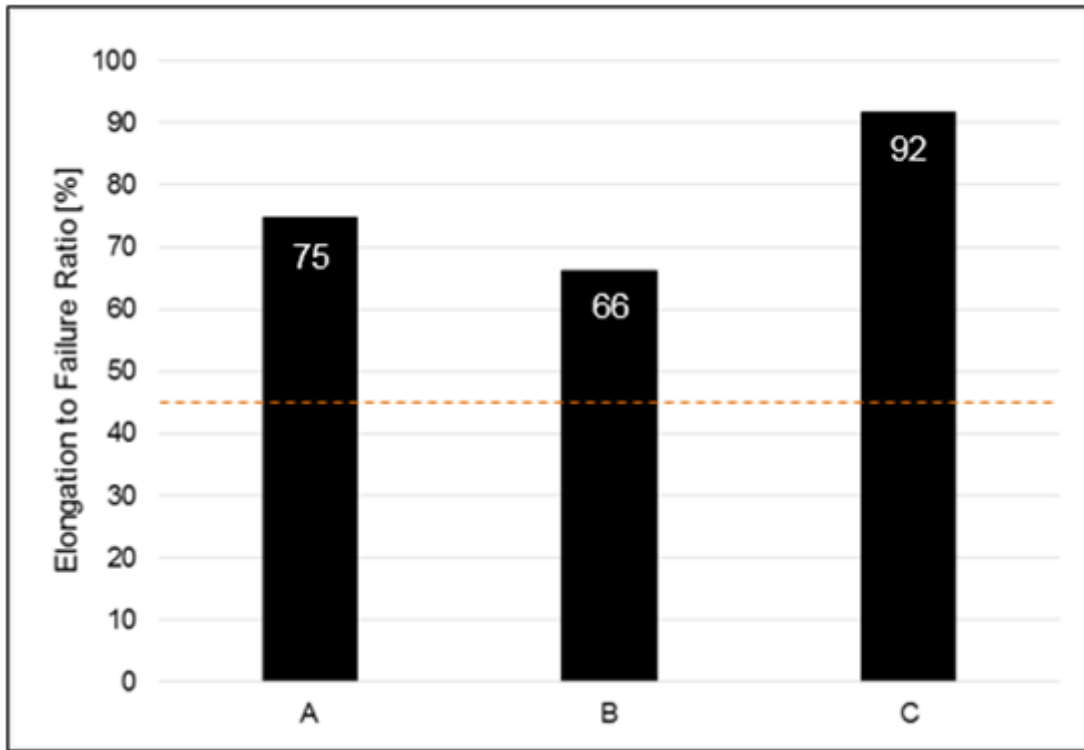
Figure 4: Elongation to Failure Ratio of Heats A, B and C. ETFR = 45% set threshold.

Table 3
HE susceptibility SSRT test results for test configuration 1

Environ-ment	Sample n.	Reduction of Area		Elongation		Time to Failure		Ultimate Tensile Strength	
		%	RAR [%]	%	EFR [%]	min	TTFR [%]	kN	UTSR [%]
Inert	A	68.0	-	24.8	-	5283	-	13	-
Aggressive	A-1	47.5	69.9	19.1	76.8	4370	82.7	13.9	107.2
Aggressive	A-2	50.0	73.6	17.1	68.8	4370	82.7	13.1	100.9
Aggressive	A-3	53.9	79.3	19.4	78.4	4680	88.6	13.1	100.7
Average			**74.3**		**74.7**		**84.7**		**102.9**

Inert	B	63.2	-	26.7	-	5560	-	11.0	-
Aggressive	B-1	65.1	103.1	18.8	70.2	4447	80	14	126.9
Aggressive	B-2	59.1	93.5	18	67.3	4310	77.5	13.4	121.2
Aggressive	B-3	51.6	81.7	16.3	61.1	3991	71.8	13.9	125.6
Average			**92.8**		**66.2**		**76.4**		**124.6**

Inert	C	76.6	-	18.6	-	4320	-	12.9	-
Aggressive	C-1	66.1	86.3	17.8	95.7	3970	91.9	13.2	102.1
Aggressive	C-2	62.8	81.9	16.5	88.4	3923	90.8	13.3	102.4
Aggressive	C-3	52.8	68.9	16.9	90.9	4006	92.7	13.5	104.5
Average			**79.0**		**91.7**		**91.8**		**103.0**

Test Configuration 2

The HE susceptibility coefficient, calculated for each material grade according to the equation (1) are presented in **Figure 5**. The HE susceptibility coefficients of all three material grades are below the set threshold of 50%, indicating good HE resistance. The lowest HE susceptibility coefficient (27%) is attributed to the Heat C (150K material designation) whereas the Heat B (140 material designation) reveals the highest susceptibility to HE (37%), although this grade is still conforming to the test approving requirements. Detailed SSRT results are summarized on **Table 4**.

SEM techniques were used to examine the outer ring of the fracture surfaces (hydrogen-affected zone), since this is the more representative region of the fracture considering the hydrogen permeation on the sample. Images of samples from Heats A, B and C are shown in **Figure 6**, **Figure 7** and **Figure 8**, respectively. The structures with zigzag shape crossing the grains indicate a typical mode of transgranular cracking morphology related to HELP-mechanism (Hydrogen-Enhanced Localized Plasticity Mechanism).
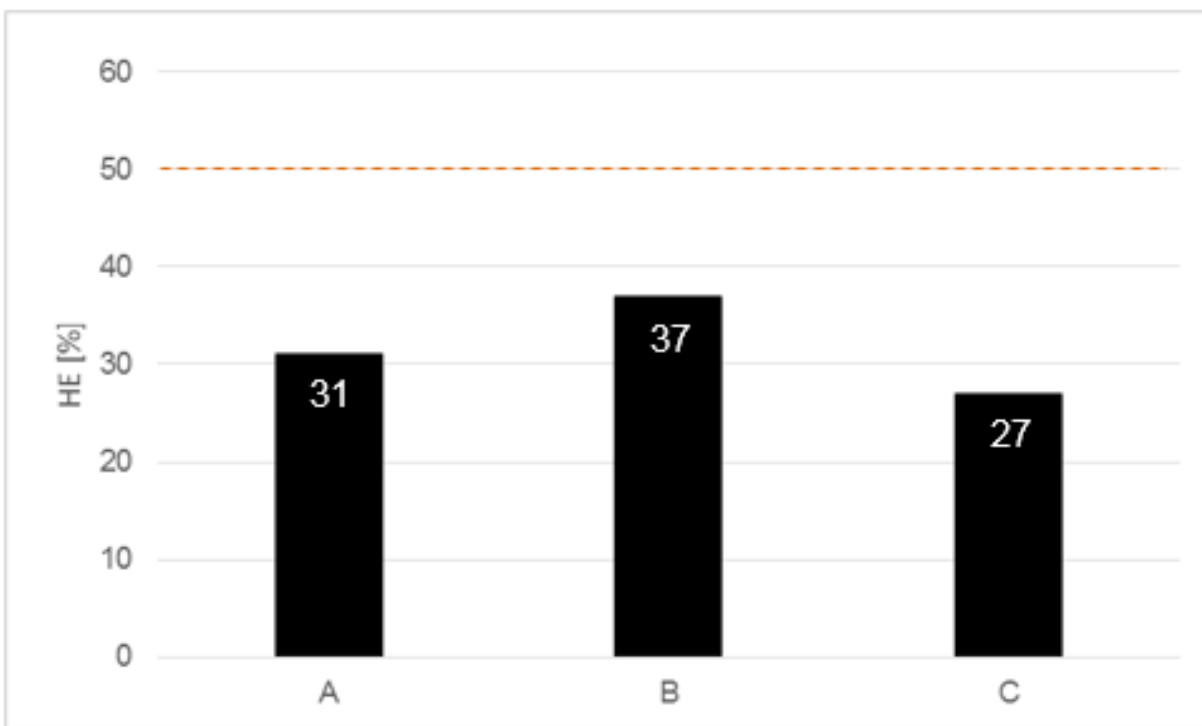

Figure 5: HE (%) of Heats A, B and C. 50% = set threshold.

Table 4
HE susceptibility SSRT test results for test configuration 2

| Environ-ment	Sample n.	Displacement		Time to failure			Ultimate Tensile Strenght	
		mm	DFR (%)	s	min	TTFR (%)	N	UTR (%)
Inert	A-2	1.20	-	215730	3596	-	23535	-
Aggressive	A-3	0.83	69.2	149280	2488	69.2	17227	73.2
Aggressive	A-4	0.80	66.4	143160	2386	61.4	17482	68.6
Aggressive	A-5	0.77	64.2	216480	3608	92.8	17752	69.6
Average			**66.6**			**74.4**		**70.5**
Inert	B-2	1.30	-	233310	3889	-	25493	-
Aggressive	B-3	0.77	59.4	138720	2312	59.5	16884	66.2
Aggressive	B-4	0.77	59.4	138600	2310	59.4	17255	67.7
Aggressive	B-5	0.80	61.8	144120	2402	61.8	17461	68.5
Average			**60.2**			**60.2**		**67.5**
Inert	C-2	1.34	-	241800	4030	-	27081	-
Aggressive	C-3	0.97	72.4	174960	2916	72.4	21030	77.7
Aggressive	C-4	0.94	70.2	169680	2828	72.7	21314	83.6
Aggressive	C-5	0.92	68.7	166080	2768	71.2	21398	83.9
Average			**70.4**			**72.1**		**81.7**
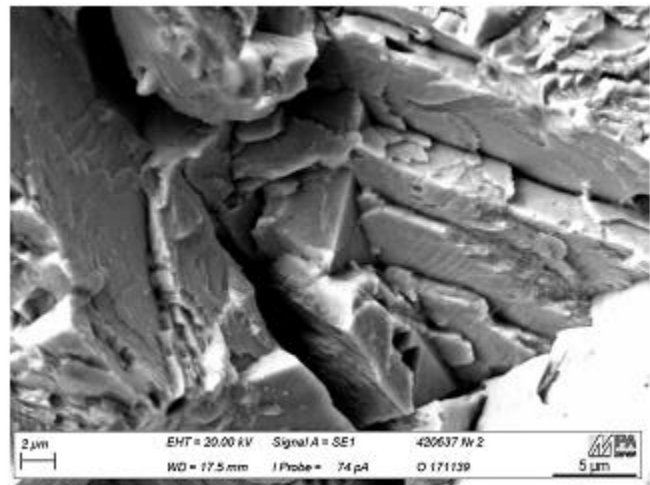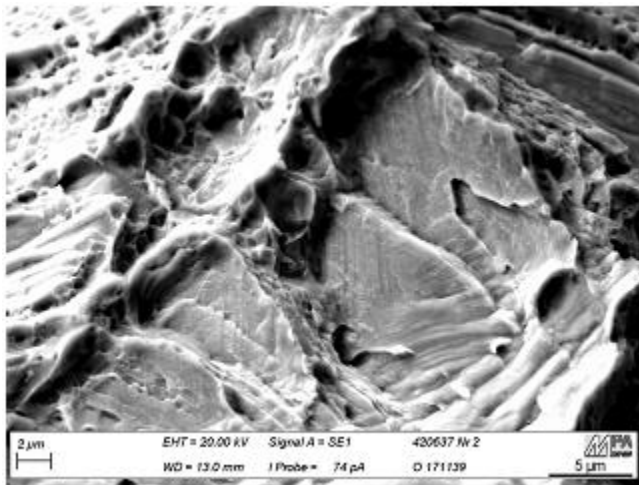
Figure 6: SEM micrographs of the outer ring of the fracture surfaces of Heat A
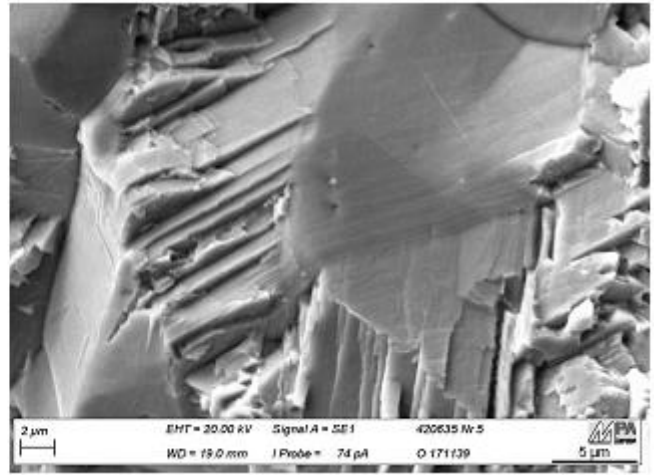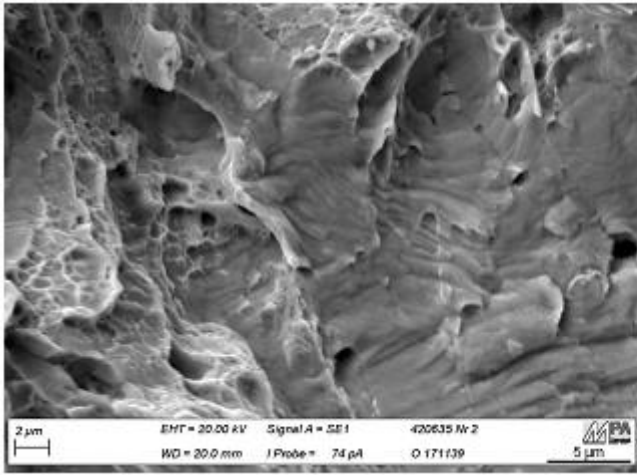
Figure 7: SEM micrographs of the outer ring of the fracture surfaces of Heat B
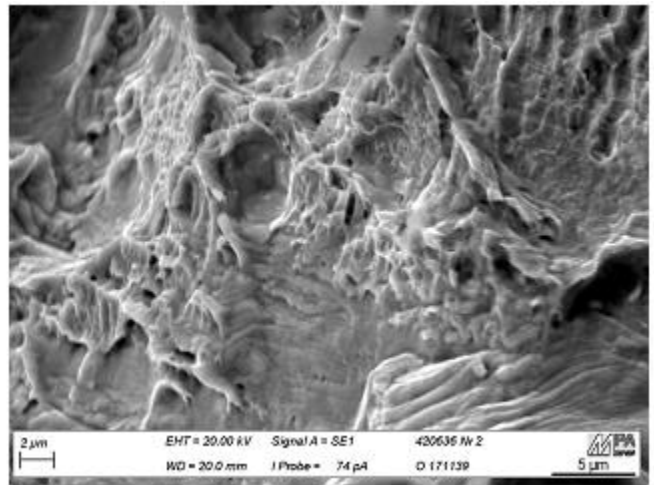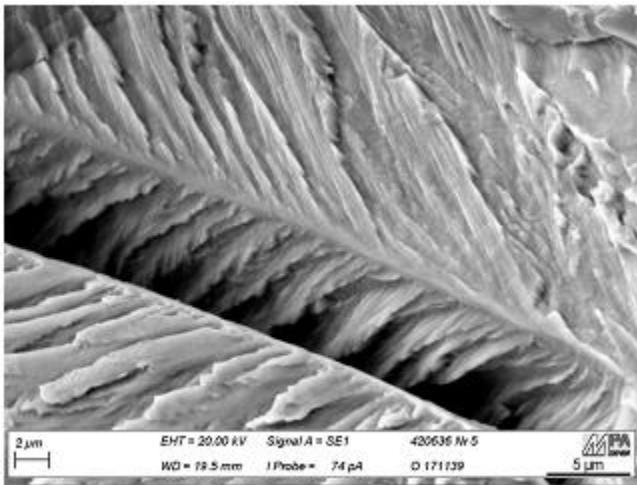
**Figure 8: SEM micrographs of the outer ring of the fracture surfaces of Heat A**

Neutron Scattering Techniques

Figure 9 shows first scattering curves of the three different samples of alloy N07718 in the different material conditions (heat treatments A, B and C) after radial averaging (despite the data shows some anisotropy and further analysis will be perform in the future). It is clearly visible that the heat treatment has strong influence on the SANS signal.

It can be seen that at room temperature heat treatment A and B show similar results, but heat treatment A presents slightly bigger precipitates (showed peak at smaller Q values) as it is expected, due to the slightly higher age hardening temperature. In contrast, the Heat C presents a very strong peak that could be ascribed to particle interaction. These precipitates should be ascribed to both γ' and γ'' precipitates and for further correlation a deep study with further methods as for example SEM has to be performed.

Figure 10 shows the three different diffraction patterns of the three different measured samples together with the expected position of the main peaks of the γ-matrix and γ' and γ'' hardening phases. From this patterns it can be seen that the three samples show similar diffraction patterns but differ slightly in the amount and perhaps the morphology of the γ'' hardening precipitates, as it can be concluded from the different shape, width and height of the peaks corresponding to this phase (especially in sample C, 150K material designation). Furthermore, only a very low volume fraction of the δ phase can be seen in these diffraction patterns regardless the heat treatment. The corresponding

Rietveld refinement patterns of these patterns provides the cell parameters and vol.% of the different phases. First obtained values are summarized in Table 5. Sample C yield to higher amount of γ' phase and also slightly higher amount of γ'', while samples A and B show similar values.
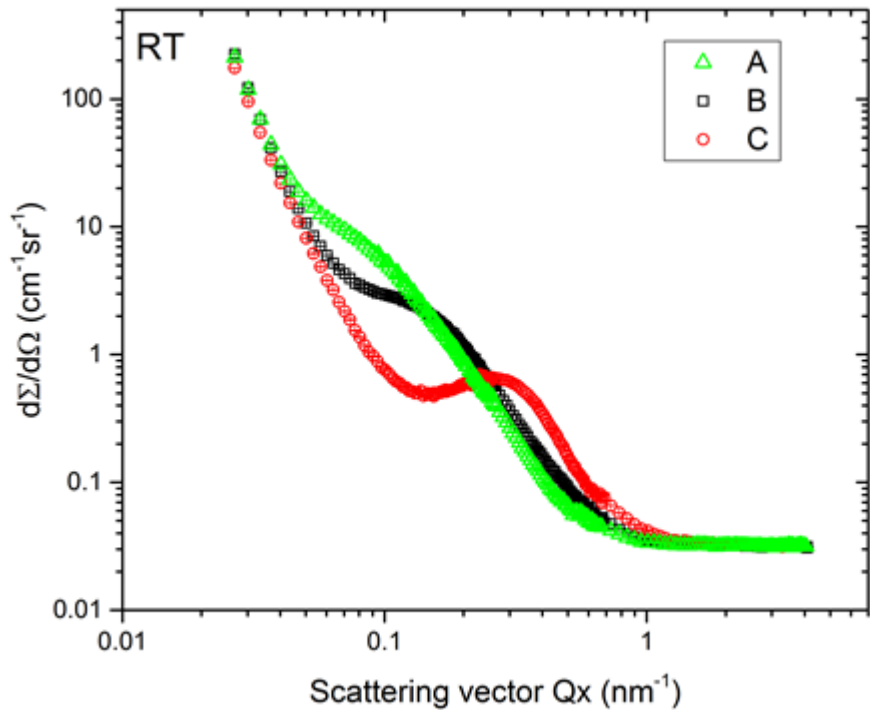
Figure 9: Fitted SANS scattering curves of Alloy N07718 at RT in different material conditions (Heats A, B and C)
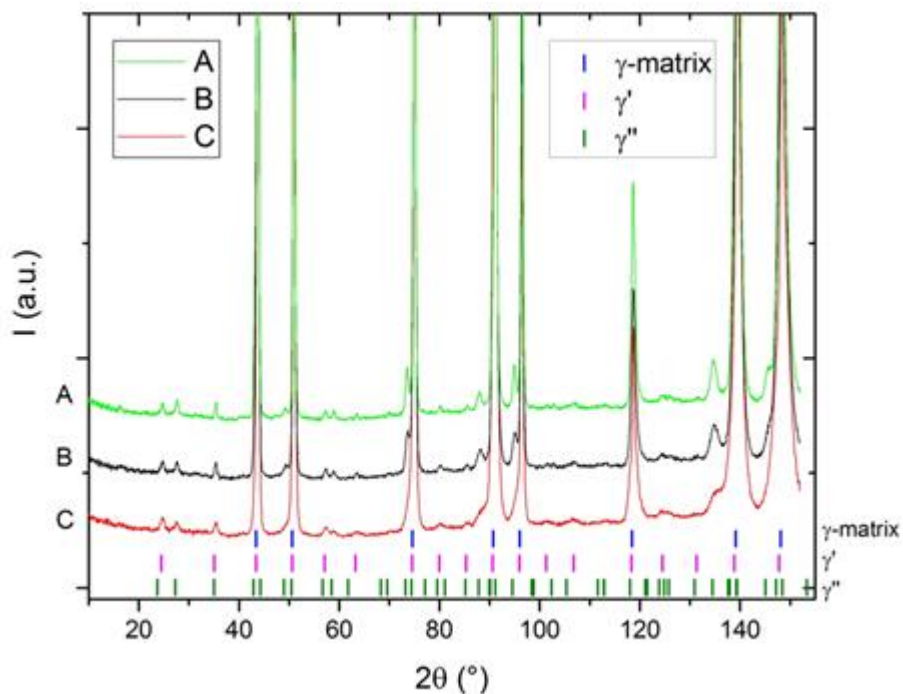
Figure 10: Neutron Diffraction patterns (from SPODI instrument) of the alloy N07718 after three heat treatments with the expected position of the main peaks of the different phases γ-matrix and the two hardening phases γ' and γ")

Table 5
Size distribution and particle volume fraction of phases of heats A, B and C of Alloy N07718 accessed by neutron scattering techniques

Heat ID	ND - Lattice parameters (Å) and weight fractions of participating phases (wt.%)			Average Particle size analysis (first approximation from Q position)
	ɣ-matrix	ɣ'-phase	ɣ"-phase	Particle size (nm)
A	a=b=c=3.60 (76.6%)	a=b=c=3.59 (13.1%)	a=b=3.60 c=7.43 (10.3%)	5
B	a=b=c=3.60 (73.6%)	a=b=c=3.60 (12.7%)	a=b=3.61 c=7.41 (13.7%)	4
C	a=b=c=3.60 (67%)	a=b=c=3.59 (19%)	a=b=3.62 c=7.25 (14%)	3.5

CONCLUSIONS

Neutron scattering methods made it possible to assess non-destructively, over a large volume of the order of 1 cm^3, information on the phase and particle size distribution of the hardening phases present in alloy N07718. The analysis is limited with SEM methods due to the fact that only very small volume can be observed but no real bulk information can be carried out.

As stated in the recent literature, the results showed that the presence of precipitates, and their distribution can directly affect the hydrogen embrittlement susceptibility and define the type of embrittlement mechanism.

When the volume fraction of each grade of Alloy N07718, obtained by neutron diffraction, is compared to the hydrogen embrittlement susceptibility showed by each grade, a relationship between the presence and distribution of the hardening phases and the interaction of the hydrogen with the microstructure can be made. The material that presents the highest volume fraction of γ'-precipitates presents the best behavior against hydrogen attack in the both applied testing methods. This corresponds to the heat-ID "C" and to the strength level of 150 ksi. The heat-ID "A" with the strength level of 120 ksi exhibits the second best behavior against hydrogen embrittlement that shows the second highest volume fraction of γ'-precipitates and a relative low volume fraction of γ''-precipitates. The heat-ID "B" with the strength level of 140 ksi has the lowest volume fraction of γ'-precipitates and a relative high volume fraction of γ''-precipitates that results in an increased susceptibility to hydrogen embrittlement.

These results lead to the interpretation that higher volume fractions of γ'-precipitates and/or lower volume fractions of γ''-precipitates have positive effects on the resistance of the material against hydrogen embrittlement. Although the ranking has been made, it is important to note that the three material grades show acceptable resistance to hydrogen embrittlement.

Further studies to better understand the relationship between hardening-phases precipitation and HE susceptibility and the mechanism of embrittlement in Alloy N07718 are being carried out and the results will be presented in a future publication.

ACKNOWLEDGEMENTS

REFERENCES

1. M. Ziomek-Moroz, "Environmentally Assisted Cracking of Drill Pipes in Deep Drilling Oil and Natural Gas Wells", Journal of Materials Engineering and Performance, 21, 6 (2012), p. 1061-1069

2. R. Kane, M. Cayard, Roles of H2S in the behavior of engineering Alloys: a Review of Literature and Experience, CORROSION/98, paper no. 274 (Houston, TX: NACE, 1998)

3. Z. Tarzimoghadam, D. Ponge, J. Klöwer, D. Raabe, "Hydrogen-assisted Failure in Nickel base alloy UNS N07718", CORROSION/2016, paper no. 7459 (Houston, TX: NACE 2016)

4. Z. Tarzimoghadam, M. Rohwerder, and 6 co-authors, „Multi-scale and spatially resolved hydrogen mapping in a Ni-Nb model alloy reveals the role of the delta phase in hydrogen embrittlement of alloy 718", Elsevier, Acta Materialia 109 (2016) 69-81

5. B. Kagay, K. Findley, S. Coryell, A.B. Nissan, "Effects of alloy 718 microstructure on hydrogen embrittlement susceptibility for oil and gas environments", Material Science and Technology Vol. 32, No 7-8 (2016): 697-707.

6. L. Liu, K. Tanaka, A. Hirose, K. F. Kobayashi, "Effects of precipitation phases on the hydrogen embrittlement sensitivity of Inconel 718," Science and Technology of Advanced Materials 3 (2002): 335-344.

7. Z. Guo, M. Zhao, C, Li, S. Chen, L. Rong, Mechanism of hydrogen embrittlement in a gamma-prime phase strengthened Fe-Ni based austenitic alloy", Elsevier, Materials Science and Engineering A 555 (2012) 77-84

8. M. C. Rezende, L. S. Araujo, S. B. Gabriel, D. S. dos Santos, L. H. de Almeida, "Hydrogen embrittlement in nickel-based superalloy 718: Relationship between γ´+ γ´´ precipitation and the fracture mode," International Journal of Hydrogen Energy 40 (2015): 17075-17083

9. O. Gosheva, G. Anderson, M. Oechsner, J. Klöwer, A. Aghajani, "Impact of microstructure on hydrogen solubility and diffusivity in UNS 07718", CORROSION/2016, paper no. 7267 (Houston, TX: NACE 2016)

10. Sarmiento Klapper H, Klöwer J, Gosheva O. 2017 Hydrogen embrittlement: the game changing factor in the applicability of nickel alloys in oilfield technology. Phil. Trans. R. Soc. A 375: 20160415.

11. S. Mühlbauer, A. Heinemann, A. Wilhelm, L. Karge, A. Ostermann, I. Defendi, A. Schreyer, W. Petry, R. Gilles, „The new small-angle neutron scattering instrument SANS-1 at MLZ-characterization and first results", Nuclear Instruments and Methods in Physics Research A 832 (2016) 297-305.

12. M. Hoelzel, A. Senyshyn, V. Baran, M.J. Mühlbauer, "SPODI High-resolution powder diffractometer" Manual of the JCNS Laboratory Course Neutron Scattering. https://wiki.mlz-garching.de/_media/fopra:tum-praktikum-spodi-2016.pdf

13. API Standard 6ACRA, First Edition (August 2015), "Age-hardened Nickel-based Alloys for Oil and Gas Drilling and Production Equipment" (Washington, NW: API Publishing Services).

14. ASTM E112-13, "Standard test Methods for Determining Average Grain Size" (West Conshohocken, PA: ASTM International)

15. NACE TM0198-2016, "Slow Strain Rate Test Method for Screening Corrosion-Resistant Alloys (CRAs) for Stress Corrosion Cracking in Sour Oilfield Service", (Houston, TX: NACE International)

16.   L. Foroni, "Hydrogen Embrittlement Susceptibility of Precipitation Hardened Ni-Alloys", CORROSION/2014, paper no. 3948 (Houston, TX: NACE, 2014).

17.   ANSI(5) NACE TM0177-2016 (latest revision), "Laboratory testing of metals for resistance to sulfide stress cracking and stress corrosion cracking in H2S environment" (Houston, TX: NACE International)

18.   O. Gosheva. Internal examination report O 17 1139.

19.   A. V. Feoktystov, H. Frielinghaus, Z. Di, S. Jaksch, V. Pipich, M.-S. Appavou, E. Babcock, R. Hanslik, R. Engels, G. Kemmerling, H. Kleines, A. Ioffe, D. Richter and T. Brückel, J. Appl. Cryst. 2015, vol. 48, pp. 61-70.

20.   http://www.qtikws.de, SANS data treatment package, accessed: 2018.

21.   J. Kohlbrecher, SASfit: a Program for Fitting Simple Structural Models to Small Angle Scattering Data, 2012.

22.   R. Gilles, B. Krimmer, H. Boysen, H. Fuess: Appl Phys A-Mater, 2002, vol. 74 (Suppl. S), pp. 148-150.

23.   M. Hoelzel, A. Senyshyn, N. Juenke, H. Boysen, W. Schmahl, H. Fuess: Detect. Assoc. Equip., 2012, vol. 667, pp. 32-7.

24.   H.M. Rietveld: J. Appl. Crystallogr., 1969, vol. 2, pp. 65-71.

25.   J. Rodríguez-Carvajal: Phys. B Condens. Matter, 1993, vol. 192, pp. 55-69.

26.   J Rosenberg, J. Klöwer, J. Groth, C. Bosch, G. Genchev, „Effect of heat treatment on mechanical properties and corrosion resistance of Nickel Alloy UNS N07718 – 140 ksi and 150 ksi grades", CORROSION/2018, paper no. 10650 (Houston. TX, 2018).

27.   U. Heubner, J. Klöwer and 5 co-authors: *Nickel Alloys and high-alloyed special stainless steels*, 4th edition (Renningen, Germany: Expert-Verlag, 2012).

28.   S. A. McCoy, S. K. Mannan, C. S. Tassen, D. Maitra, J. R. Crum, "Investigation of the effect of Hydrogen on High Strength Precipitation Hardened Nickel alloys for O&G service," CORROSION/2015, paper no. 5911 (Houston, TX: NACE, 2015).

29.   A., Devaux, l. Nazé, R. Molins, A. Pineau, "Gamma double prime precipitation kinetic of Alloy 718," Materials Science and Engineering A 486 (2008): 117-122.

30.   B. Kagay, K. Findley, S. Corywell, A. Nissan, "Slow Strain Rate and Step Load Hydrogen Embrittlement Testing of UNS N07718," CORROSION/2016, paper no. 7861 (Houston, TX: NACE, 2016).

31.   J. Kloewer, H. Sarmiento-Klapper, O. Gosheva, Z. Tarzimoghadam, "Effect of Microstructural Particularities on the Corrosion Resistance of Nickel Alloy UNS N07718 – What really makes the Difference," CORROSION/2017, paper no. 9068 (Houston, TX: NACE, 2017).

32.   W. Huang, W. Sun, A. Samson, D. Muise, „Investigation of Hydrogen Embrittlement Susceptibility of Precipitation hardened Nickel Alloys under Cathodic Protection Condition", CORROSION/2014, paper no. 4248 (Houston, TX: NACE, 2014).

---

[5] Approved American National Standard (ANSI)